High-redshift Gamma-Ray Bursts: Cosmological Applications

Eloisa Bentivegna

Department of Physics, Pennsylvania State University, University Park, PA 16802

bentiveg@phys.psu.edu

ABSTRACT

In the past forty years, Gamma-Ray Bursts have constituted a challenge and a promise both from the theoretical and from the observational standpoint. On one hand, their prompt localization, the identification of their progenitors and the details of the emission mechanism have long constituted an astrophysical enigma. On the other hand, their high-redshift detectability and tight connection with stellar formation render them a favorite candidate to probe the properties of the early universe, from its geometry and matter content to the growth of primordial perturbations. In this paper, we will describe the potential for cosmological applications of GRB data and summarize the prospectives and the problems connected with such applications.

1. Introduction

Since their discovery in the late 60s, Gamma-Ray Bursts (GRBs) have constituted a challenging astrophysical phenomenon. In the first place, the short burst duration (usually of the order of a few seconds) made localization a difficult task. In the second place, once a redshift was estabilished, the bursts appeared to be extremely energetic events, with a highly non-thermal photon spectrum, and a γ-ray component well brighter than any other observed γ-ray source. Viable progenitors and the energy extraction mechanisms were therefore at the center of intensive investigation. Third, GRBs appear to have a bimodal time distribution, with about one third of the bursts with duration $t < 2\,\mathrm{s}$ and the rest with $t > 20\,\mathrm{s}$, hinting at the existence of at least two different production mechanisms.

Many more properties render GRBs a unique phenomenon. In this report, we will only describe those GRBs' features that are relevant to cosmology. With a significant (and steady growing) sample of bursts beyond $z \sim 1$, and a concrete possibility of detection beyond $z \sim 10$, GRBs are probably the most distant events we can observe today. This feature, in addition to several other desirable properties, makes GRBs particularly suitable to probe the very high-redshift universe.

In section 2 we will give a detailed analysis of the GRB properties that are most relevant from the cosmological standpoint, and in section 3 and we will describe how these properties can be used to gain information on the structure and composition of the universe in the early epochs.

2. Properties of Gamma-Ray Bursts

Two main factors render GRBs particularly suitable for the study of the high-redshift universe: first, their exceptional luminosity in the γ-ray band pushes GRB detectability up to $z \sim 30$; second, the production mechanism tightly connects these events to star formation, thereby making them an optimal probe to observe early stellar dynamics. In this section, we will analyze these two properties individually in order to highlight their respective roles in the cosmological applications of GRB data.

2.1. Detectability

The first task to be accomplished in order to discuss the cosmological potential of GRBs is to evaluate their degree of detectability in all emission bands. We will report on two separate analyses, the first involving the detectability of the burst itself and the second involving the detectability of the afterglow. One important issue when dealing with distant objects is the procedure to measure their redshift, and we will also report on this topic at the end of this section.

2.1.1. Bursts

As a first estimate, the maximum redshift z_{max} at which each specific GRB is detectable is given by the condition that its peak photon flux:

$$P(z) \equiv \int_{\nu_l}^{\nu_u} \frac{dP}{d\nu} d\nu \tag{1}$$

equal, at $z = z_{max}$, the detector sensivity:

$$P(z_{max})a = P_{det} \tag{2}$$

where a is the detecting area, and ν_l, ν_u represent the lower and upper limit on the frequency band of observation. If we set:

$$L_P \equiv \int_{\nu_l}^{\nu_u} \frac{dL_P}{d\nu} d\nu \tag{3}$$

where $dL_P/d\nu$ is the photon number spectrum of the source, then the number of photons emitted per unit time in the source frequency interval $[\nu_u(1+z), \nu_l(1+z)]$ is given by:

$$\frac{\text{number of photons in } [\nu_u(1+z), \nu_l(1+z)]}{\text{unit of (source) time}} = \frac{L_P}{(1+z)^{\alpha-1}} \tag{4}$$

where α expresses the frequency dependence of the photon number spectrum, $dL_P/d\nu \propto \nu^{-\alpha}$. Those photons are going to reach the detector within a time interval given by $a_0/a = 1+z$, so that the number of photons per unit area and per unit time detected on Earth is given by:

$$P(z) = (1+z)^{-1} \frac{L_P/(1+z)^{\alpha-1}}{4\pi(a_0 r)^2} \tag{5}$$

r representing the coordinate distance to the source (and $a_0 r$ being therefore the proper distance). Remembering that the distance luminosity $d_L(z)$ is defined as:

$$d_L(z) = a_0 r(1+z) \tag{6}$$

we finally have:

$$P(z) = \frac{L_P}{4\pi d_L^2(z)(1+z)^{\alpha}} \tag{7}$$

Lamb & Reichart (2001) have performed this analysis on a flat model, where:

$$d_L(z) = \frac{c}{H_0} \int_0^z \frac{d\zeta}{\sqrt{\Omega_M(1+\zeta)^3 + \Omega_\Lambda}} \tag{8}$$

Taking into account the detector sensitivity of both BATSE/HETE-2 and *Swift*, they have produced the plot in Fig. 1. Their choice for the cosmological parameters, as well as the detection thresholds for the different experiments are listed in Table 1.

From inspection of Fig. 1, it is clear that, due to their extremely high luminosity and due to the almost complete transparency of the IGM to $\gamma-$rays, GRBs are detectable, if present, out to redshifts of a few tens.

Table 1. Parameters in the detectability analysis of Lamb & Reichart (2001)

Parameters	Values in Lamb & Reichart (2001)
Ω_M	0.3
Ω_Λ	0.7
H_0	65 $\mathrm{km\,s^{-1}\,Mpc^{-1}}$
P_{det}^{B-H2}	0.2 $\mathrm{ph\,s^{-1}}$
P_{det}^{Swift}	0.04 $\mathrm{ph\,s^{-1}}$

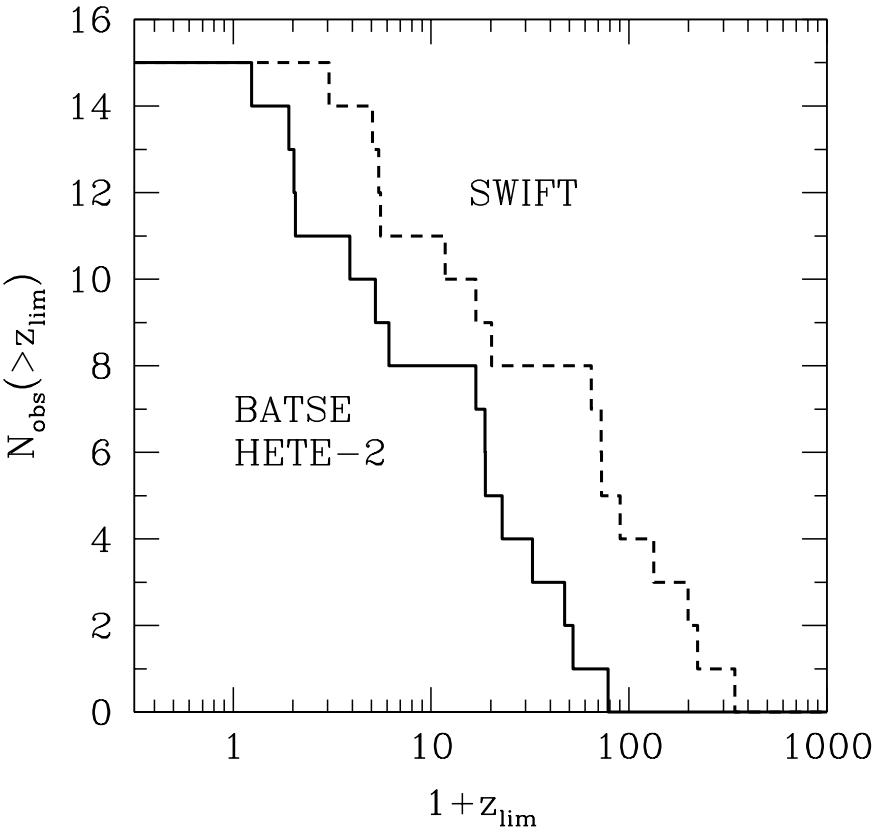

Fig. 1.— Number of GRBs (out of a sample of 15 bursts) detectable at redshift z, from Lamb & Reichart (2001).

2.1.2. Afterglows

A somewhat more refined analysis (Gou et al. (2004)) involves a calculation of the flux of the afterglow in the IR and X-ray bands (i.e., those less affected by extinction), with the appropriate correction due to galactic and extragalactic photoabsorption along the line of sight, and a full treatment of both the forward shock and the reverse shock contribution to the flux.

Fig.2 shows a typical K-band lightcurve for a burst located at $z = 1$. The solid line represents the forward shock contribution, whereas the dashed one is the reverse shock. Manifestly, the flux associated with the latter is negligible at late times, but does play an important role earlier on. The reverse shock is therefore expected to have a comparatively heavier weight for higher redshift bursts, since time intervals are dilated by a factor $1 + z$, implying that fixed observer times correspond to earlier times for more distant bursts.

The results of this analysis are shown in Fig. 3. The lines with superimposed symbols represent the forward shock, the ones without symbols, the reverse shock. The curves are calculated at observer time equal to 10 minutes (solid), 2 hours (dashed) and 1 day (dotted), and the detection threshold represent ROTSE at very early times (dashed) and very late times (solid) for the V band, and the James Webb Space Telescope for the K and M bands.

Despite the different scenario involved, the results are not qualitatively distant from the ones obtained for γ-ray emission: GRB and their afterglows appear to be detectable up to very high redshift, $z \sim 30$.

2.1.3. Measuring the redshift

There are essentially two methods to measure a GRB's redshift:

(i) Measuring the reshift of the absorption lines in the GRB afterglow. Strictly speaking, the measured redshift is not the GRB's, but the one of the first absorber system encountered along the line of sight. Thus, This method only provides a lower limit, although the first absorber system is usually pretty close to the GRB itself, often the host galaxy itself. Although Balmer lines are redshifted out of the optical bandwidth for any redshift greater than about 5, metal lines might still be detectable. GRB location in star forming regions ensures, even at early epochs, a sufficiently high metallicity to make the equivalent widths of, say, Mg II and Fe II large enough to be detected.

(ii) Measuring the redshift of the host galaxy: this second method gives a somewhat more

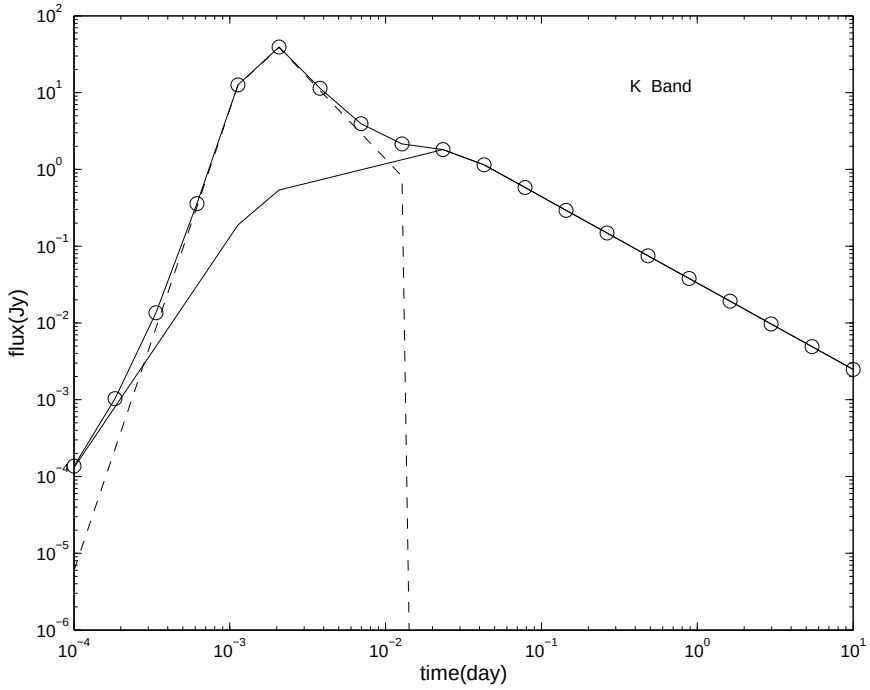

Fig. 2.— Typical K-band light curve for a GRB afterglow at $z = 1$, from Gou et al. (2004). The solid line represents the forward shock contribution, whereas the dashed line represents the reverse shock. The line with symbols is the superposition of the two components.

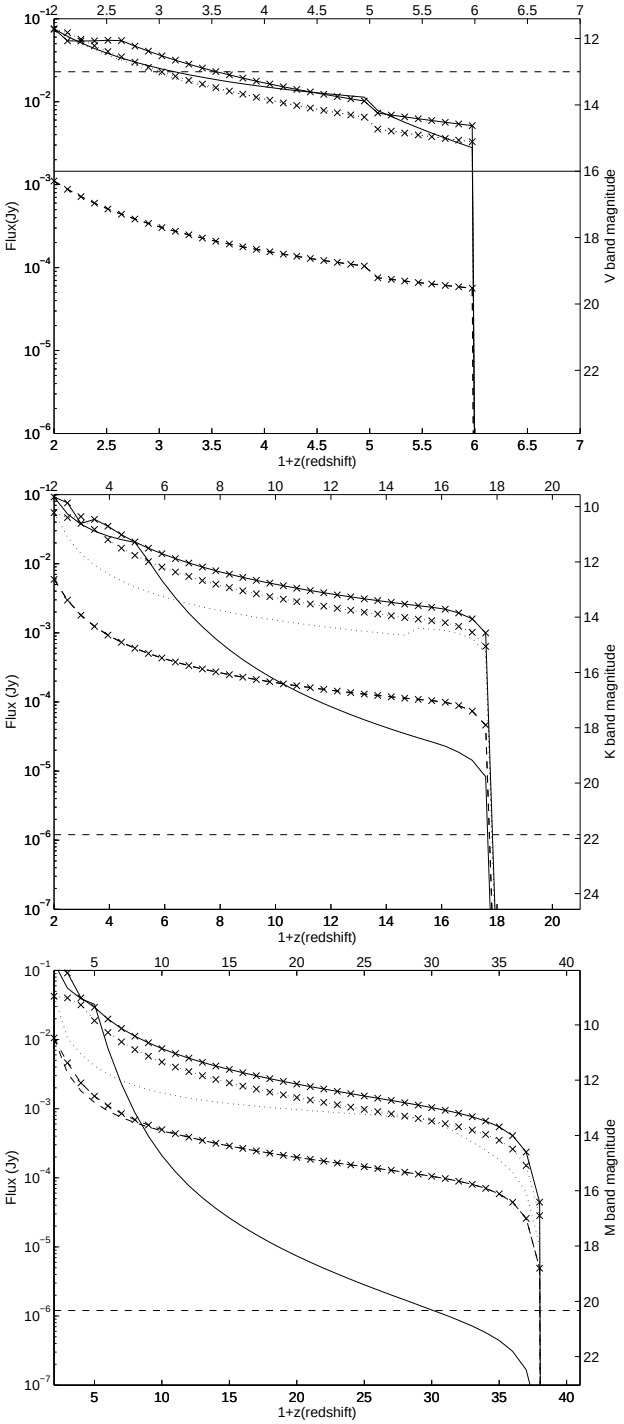

Fig. 3.— Afterglow flux in the V, K and M band, from Gou et al. (2004). Lines with symbols represent the forward shock, while those without symbols represent the reverse shock. The plots show the flux at different observation times (*solid*: 10 minutes, *dashed*: 2 hours and *dotted*: one day).

stringent estimate of the redshift, but of course entails a positional coincidence determination between the galaxy and the burst, which could be a non-trivial task. Also, the method clearly doesn't work for higher redshifts, $z \sim 5$, where galaxies are globally less massive and less bright, their luminosity decaying as $(1+z)^4$.

Clearly, each method has its own drawbacks, and the redshift measure is more accurate if more than one estimate is available. Finally, it is worth mentioning that the recent proposal of a calibration procedure that reduces the luminosity dispersion of GRBs (see section 3.1 below) has made it possible to give an estimate of L and calculate z thereof, using measures of the absolute luminosity $l(z)$.

2.2. Origin

Several, independence pieces of evidence point at massive star collapse as the production mechanism of the long-duration GRBs:

- A GRB-supernova connection has been estabilished for at least one case (GRB 030329 - SN 2003dh, Fig. 4), and in several other instances a correspondence is also likely. The detectability of SNe at the typical GRB redshift ($z \sim 1$) is extremely reduced, especially if the lightcurve is superimposed to the burst's. Nonetheless, color changes in the optical afterglow at late times and deviations from the typical powerlaw light curve of can signal the presence of a SN component (Stanek 2004). It is to be noted that the supernovae in question are typically core collapse supernovae, i.e. type Ib/Ic, thereby strengthening the hypothesis of a star collapse generation for the long GRBs;

- In some cases, the identification of the GRB host galaxy and the analysis of its color revealed that GRBs occur in those regions where star formation is most copious. This indirectly points at a massive progenitor, since the short lifetime of massive objects gives them a lesser chance to escape the region where they were formed before collapse (Lamb (2000)). Incidentally, this is another element favoring the *collapsar* model (central object with an accretion torus) of long GRBs over the *supranova* model (NS-NS merger) for long GRBs, since binary mergers are expected to take place well outside the region of formation.

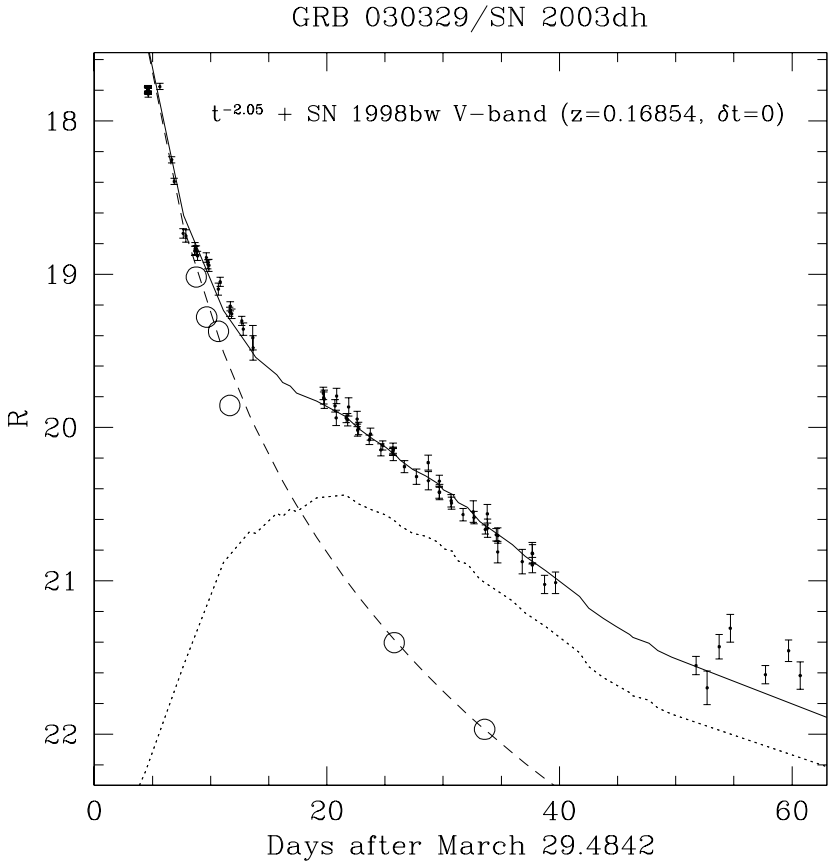

Fig. 4.— The optical transient light curve for GRB 030329 in the R-band (solid line) and its decomposition into the GRB, powerlaw contribution (dashed) and the SN lightcurve (dotted), from Matheson (2003). The SN template has been constructed from the model V-band light curve of SN 1998bw, stretched by $(1 + z) = 1.1685$ and shifted in magnitude. The GRB afterglow continuum has been fitted to the data points (open circles) from spectral analysis.

3. Gamma-Ray Bursts as Cosmological Tools

3.1. GRBs as discriminators of cosmological models

One of the properties of Friedmann-Robertson-Walker universes is that, given an object of a certain (known) instrinsic luminosity or angular diameter, its apparent luminosity or angular diameter will depend, other than on its distance from the observer, also on the matter content (and, possibly, cosmological constant) of the universe. This is a fundamental property of all cosmologies based on general relativity: geometry governs the trajectories of light rays, and, by Einstein's equations, is shaped by the energy content of the universe.
In a Robertson-Walker universe:

$$ds^2 = -dt^2 + a^2(t)[\frac{dr^2}{1-kr^2} + r^2(d\theta^2 + \sin^2\theta d\phi^2)] \tag{9}$$

with the origin on terrestrial observers, the physical distance to an object is given by:

$$D(t) = a(t)r \tag{10}$$

However, due to cosmic recession and to the finite propagation speed of light, it is more convenient (and more useful for practical purposes) to introduce other measures of distance, based on light propagation. One possible choice is to define the luminosity distance d_L as:

$$d_L = \left(\frac{L}{4\pi l}\right)^{1/2} \tag{11}$$

where L is the intrinsic luminosity of an object and l is the apparent luminosity as seen from the observer. Obviously, in a Euclidean, nonexpanding space-time, d_L represents the real, physical distance of the object from the observer. In the spacetime (9), the following relation holds:

$$d_L(z;\Omega_{\rm M},\Omega_\Lambda) = D(t)(1+z)^2 = (1+z)\frac{c}{H_0}S_k\left[\int_0^z \frac{dz}{\sqrt{\Omega_{\rm M}(1+z)^3 + \Omega_\Lambda - (1-\Omega_{\rm M}-\Omega_\Lambda)(1+z)^2}}\right] \tag{12}$$

where

$$S_k(x) = \begin{cases} \sin x & k=1 \\ x & k=0 \\ \sinh x & k=-1 \end{cases}$$

Assuming a class of monoluminous sources (i.e., sources with all the same L), $l(z)$ will then only be a function of redshift, parametrized by the cosmological parameters $\Omega_{\rm M}$, Ω_Λ. With a catalog of (z_i, l_i) data pairs, it is then possible to compare the theoretical expectation to observations, and fit $\Omega_{\rm M}$ and Ω_Λ accordingly.

The question then arises whether GRBs constitute such a class of monoluminous sources (*standard candles*). A recent analysis (Ghirlanda, Ghisellini & Lazzati (2004)) shows that, although the intrinsic luminosity of GRBs seems to have a certain non-negligible dispersion around the mean, this dispersion can be greatly reduced by performing a "calibration" on the bursts' total γ-ray energy E_γ based on the peak energy E_{peak}. In Fig. 5, E_{peak} is plotted vs. the isotropic E_γ, on the right, and vs. the collimation-corrected E_γ (which already shows a smaller dispersion) on the left. The straight line fitting the collimation-corrected energies is given by:

$$E_{peak} \propto E_\gamma^{0.7} \tag{13}$$

and this is the calibration relationship used in the cosmological analysis. Fig. 6 estimates the adherence of the bursts to the prescribed relation.

Once the task of finding L has been accomplished, the apparent luminosity-redshift relation can be employed to constrain the cosmological parameters. In general terms, with a set of data pairs (z_i, l_i) (redshift and flux), the standard χ^2 function can be constructed:

$$\chi^2(\Omega_M, \Omega_\Lambda) = \frac{1}{M} \sum_{i=1}^{N} \frac{(l_i - l(z_i; \Omega_M, \Omega_\Lambda))^2}{\sigma_i^2} \tag{14}$$

where N is the number of bursts, M the number of degrees of freedom, and

$$l(z; \Omega_M, \Omega_\Lambda) = \frac{L}{4\pi d_L^2(z; \Omega_M, \Omega_\Lambda)} \tag{15}$$

The function $\chi^2(\Omega_M, \Omega_\Lambda)$ is then minimized in the $(\Omega_M, \Omega_\Lambda)$ plane to find the best-fit estimate of the parameters, whether the errors are calculated by plotting the confidence regions (obtained from the standard χ^2 probability) and projecting them onto the two axes.

This task has been carried out in Ghisellini (2004), whose results are shown in Figs. 7 and 8. Obviously, the GRB data alone cannot provide a tight constraint for the $(\Omega_\mathrm{M}, \Omega_\Lambda)$ pair, but if they are crossed with data from other sources (SNe, CMS), they can help reduce the extension of confidence regions and shrink the error on the fit values. In agreement with other independent data coming from SNe Ia and CMB, GRBs seem to favor a cosmological model where Dark Energy constitutes a large fraction of the matter-energy content of the universe, and Ω_M is of the order of a few tenths. Flat models are also well within the $1\,\sigma$ confidence region.

Furthermore, given the large redshift span of the bursts, one can reasonably hope to use them for more ambitious purposes, like probing the equation of state of Dark Energy. For instance, one can assume a relation like:

$$p = (w_0 + w'z)\rho \tag{16}$$

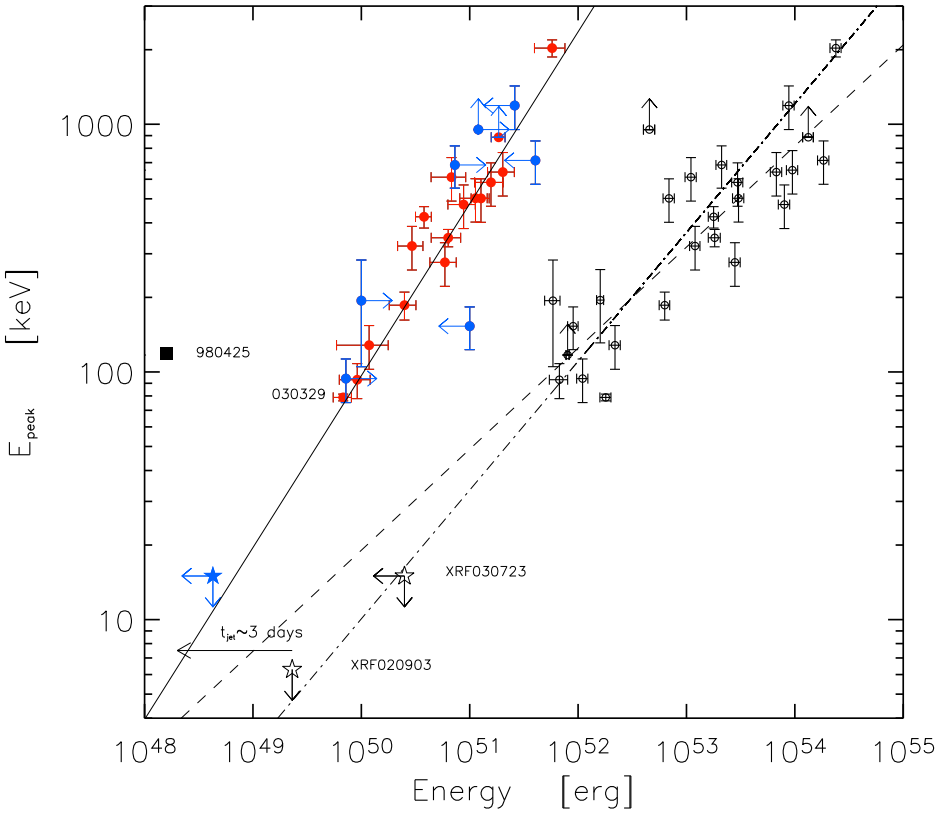

Fig. 5.— Possible calibration relation between E_{peak}, the burst peak energy, and E_γ, the total energy in the γ-band. The points on the right represent E_γ under the assumption that emission is isotropic. The ones on the left represent the collimation-corrected energy $E_\gamma(1 - cos\theta)$, θ being the jet opening angle as inferred from the achromatic break in the afterglow light curve (Ghirlanda et al. (2004)).

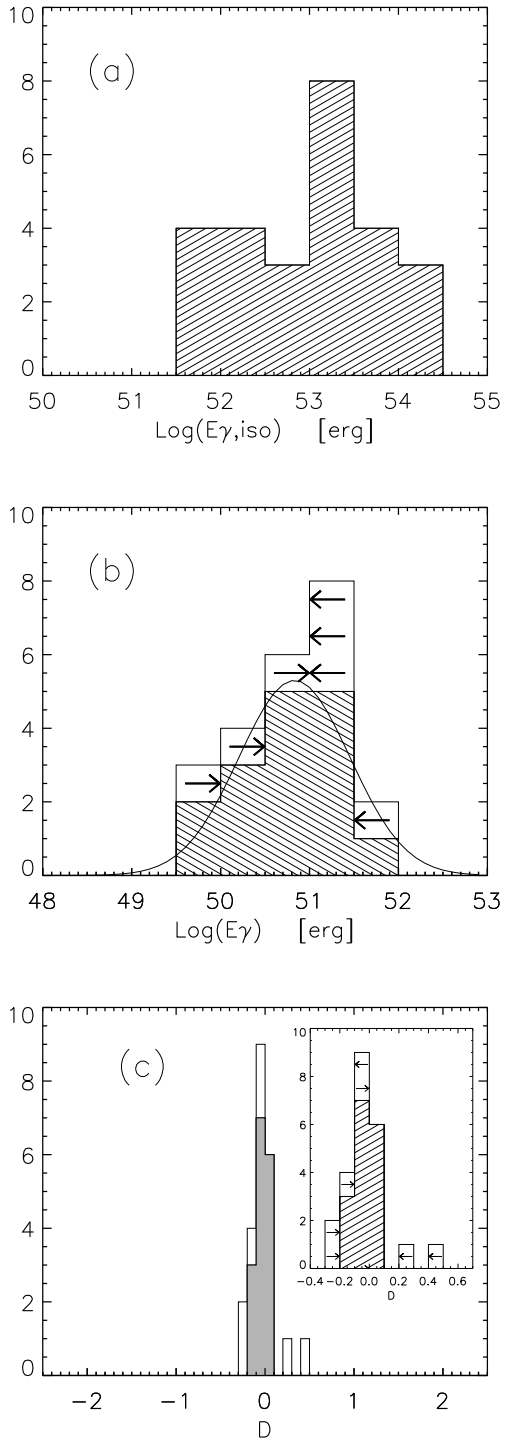

Fig. 6.— Top: distribution of the isotropic E_γ for the GRB sample in Ghirlanda et al. (2004). Center: distribution of the collimation-corrected E_γ. Bottom: distance of each burst from the correlation $E_{peak} \propto E_\gamma^{0.7}$.

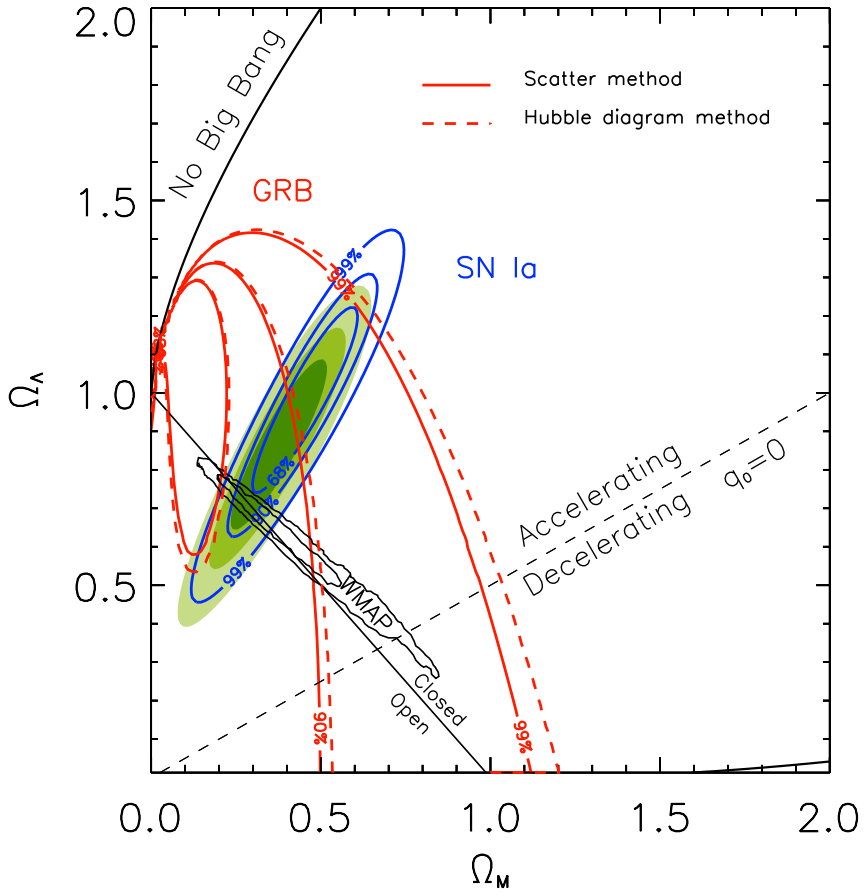

Fig. 7.— χ^2 analysis and parameter fit in the $(\Omega_{\rm M}, \Omega_\Lambda)$ plane, from Ghirlanda et al. (2004).

which will modify the time dependence of the scale factor and, consequently, the luminosity distance, which now reads:

$$d_L(z;\Omega_{\rm M},\Omega_\Lambda,w_0,w') = \\ = (1+z)\frac{c}{H_0}S_k\left[\int_0^z \frac{dz}{\sqrt{\Omega_{\rm M}(1+z)^3+\Omega_\Lambda(1+z)^{3(1+w(z))}-(1-\Omega_{\rm M}-\Omega_\Lambda)(1+z)^2}}\right] \quad (17)$$

Fitting the parameters w_0 and w' against the same data in Fig. 7, one obtains the results in Fig. 8. The ordinary, cosmological constant equation of state $w_0 = 1, w' = 0$ is still favored, but the confidence regions now extend to other possible values.

3.2. GRB rate as a probe for Stellar Formation Rate

If GRBs are actually the end result of the collapse of massive stars, it is not unconceivable to expect that the GRB rate be proportional to the Stellar Formation Rate. In this note, one can hope to trace, or at least constrain, the SFR up to very high redshift. With the estimated formation of the first objects in the universe at a redshift $z \sim 18$, and a GRB detectability that can easily reach $z \sim 30$, it is realistic to hope that GRBs shed light on the formation of structure in the early universe, on the rate at which stars and galaxies are formed, and, therefore, on the details of such formation.

With this in mind, Porciani & Madau (2000) have calculated the predicted GRB rate R_{GRB} for different SFR models, producing Figs. 9 and 10. Actual data will therefore favor or disfavor each single prediction and provide a discrimination of different theoretical models of star formation.

3.3. GRBs as a probe of metallicity evolution

An interesting open chapter of our universe is the metallicity history, i.e. how the metal content of stars, galaxies and IGM evolved from the early values inherited from primordial nucleosynthesis to the present, fully solar values. Theoretical models of star formation indicate the existence of a first generation around $z \gtrsim 15$, followed by another increase in the Star Formation Rate around $2 \lesssim z \lesssim 10$, thereby supporting a relatively high metallicity already around $z \sim 5$. However, this conclusion is not confirmed by observations of damped Ly-α (LDA) absorbers in the spectra of quasars (see Fig. 11). Lu et al (1996), for instance, have shown that there is evidence for a marked metallicity dip around $z \sim 3$.

There are several possible resolutions of this inconsistency: for instance, as illustrated in

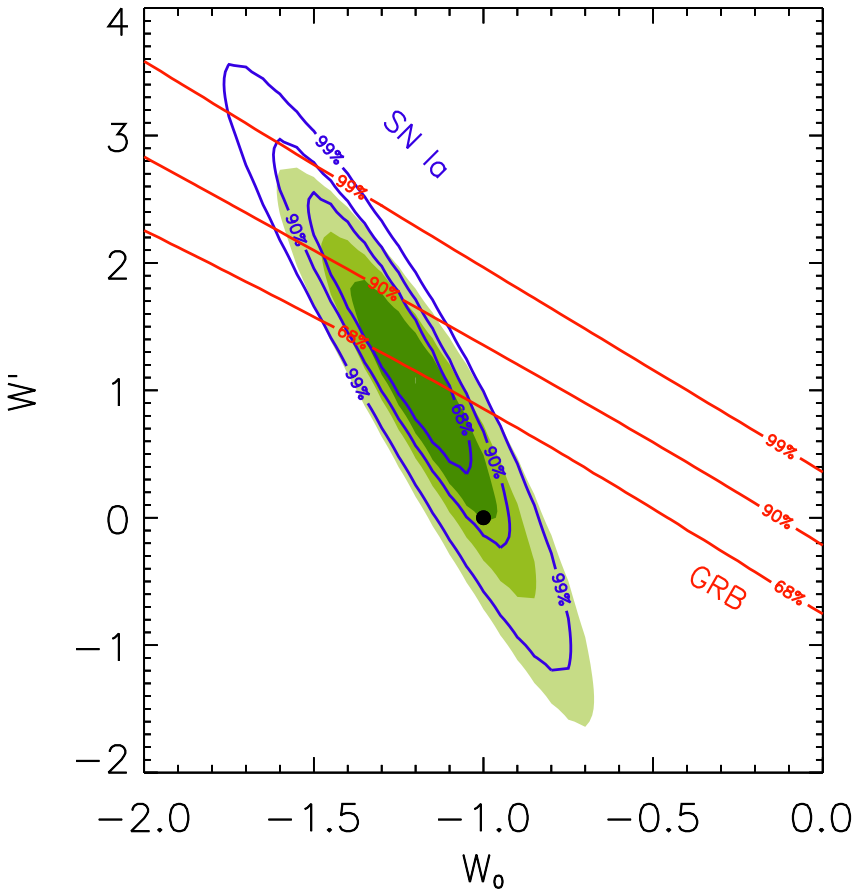

Fig. 8.— Same analysis as in Fig. 7, but in the (w_0, w') plane.

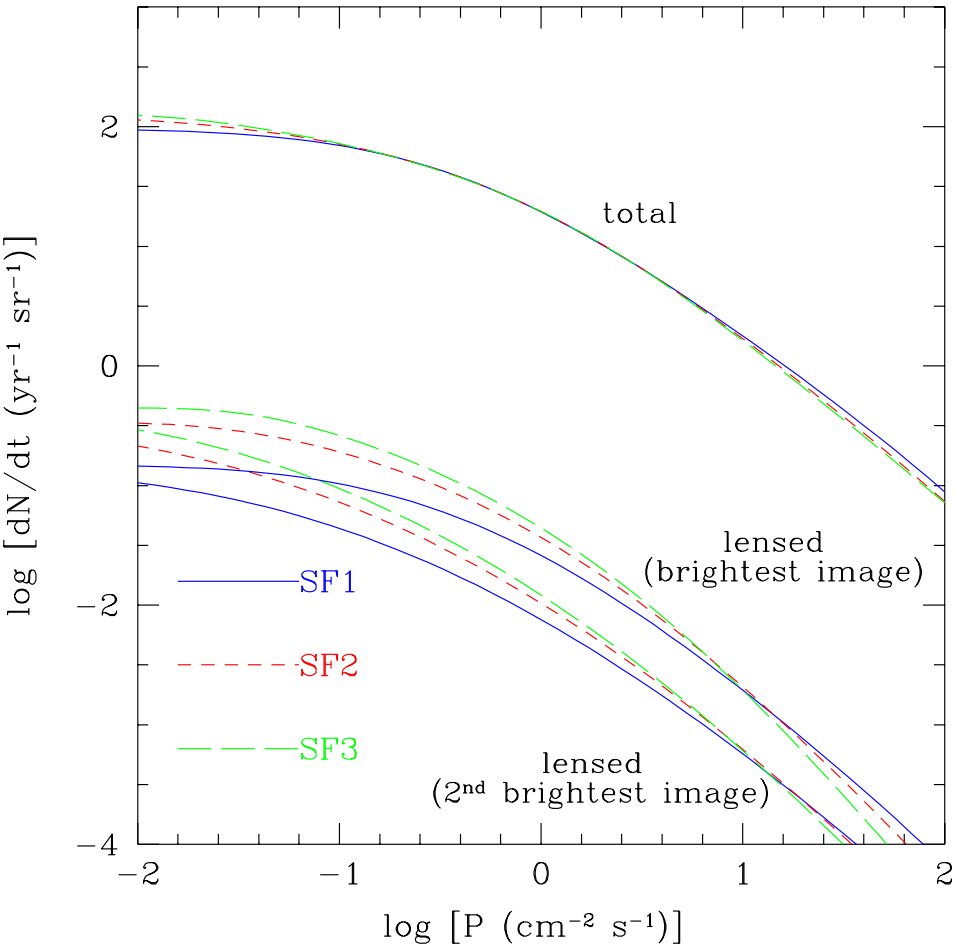

Fig. 9.— Different predictions for R_{GRB}, based on three SFR profiles (Porciani & Madau (2000)).

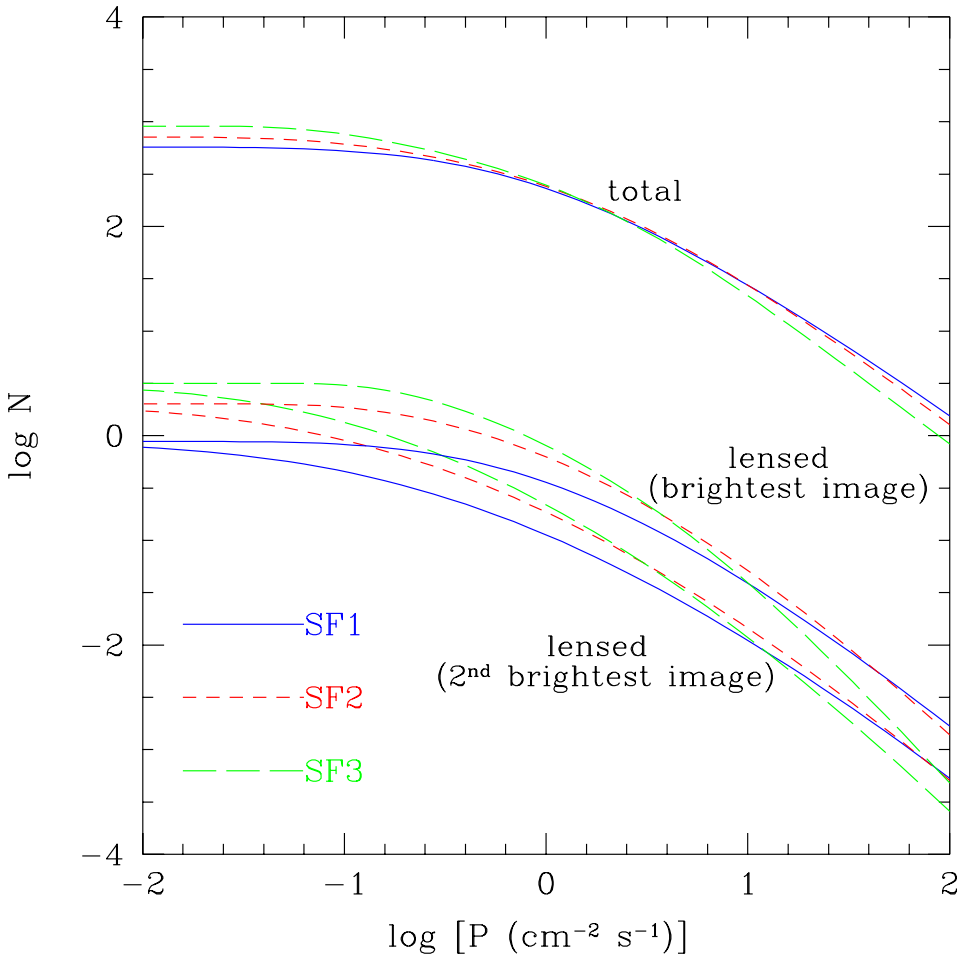

Fig. 10.— Same profiles as in Fig. 9, but plotting the total number counts for Swift during three years of observations (Porciani & Madau (2000)).

Fig. 11, metallicity is often highly non-uniform, increasing in the proximity of star-forming regions and being minimum in galactic halos and IGM. Obviously, direct observational access to the redshift interval $10 \lesssim z \lesssim 20$ can provide the ultimate answer.

Furthermore, given the GRBs/SNe connection, observations of GRBs can not only provide information on the history of metal production in our universe, but can also furnish hints regarding the mechanisms of production. As an example, it is currently estabilished that nucleosynthesis in core collapse SNe (the ones related to GRBs) is significantly different from that occurring in thermonuclear SNe. A direct observation can thus provide a description of the relative roles of the two different types of SNe in the metal enrichment of the universe.

3.4. GRBs as a probe of Large Scale Structure

Another consequence of the expected VHR detectability of GRBs is the viability of Large Scale Structure observations at redshifts much higher than those probed by QSO and galaxies. In addition, γ-rays travel essentially undisturbed through the Milky Way, permitting a homogeneous detection of the bursts.

However, the statistics associated with GRB detection are not particularly favorable to extensive LSS surveys: the expected samples will be of the order of ~ 1000, well below the analogous surveys performed by, e.g., the Sloan Digital Sky Survey.

Nevertheless, analysis of GRB afterglows, especially in terms of metal absorption lines, can help mapping the clustering of matter on the early universe. Experience from QSO absorbers has indeed shown that systems along the line-of-sight, which showed metal absorption lines, are often detected in the vicinity of galaxies. It is therefore reasonable to assume that the absorption takes place in galactic environments, thereby making such systems an interesting tracer of the distribution of matter at very high redshifts.

A systematic study of LSS can then address fundamental questions regarding the formation of structure in the early universe, and help define the features of the initial perturbation spectrum.

3.5. GRBs and reionization

The presence and detectability of very high redshift gamma-ray bursts provides a unique insight into early cosmic epochs, especially regarding the reionization era. It is well known

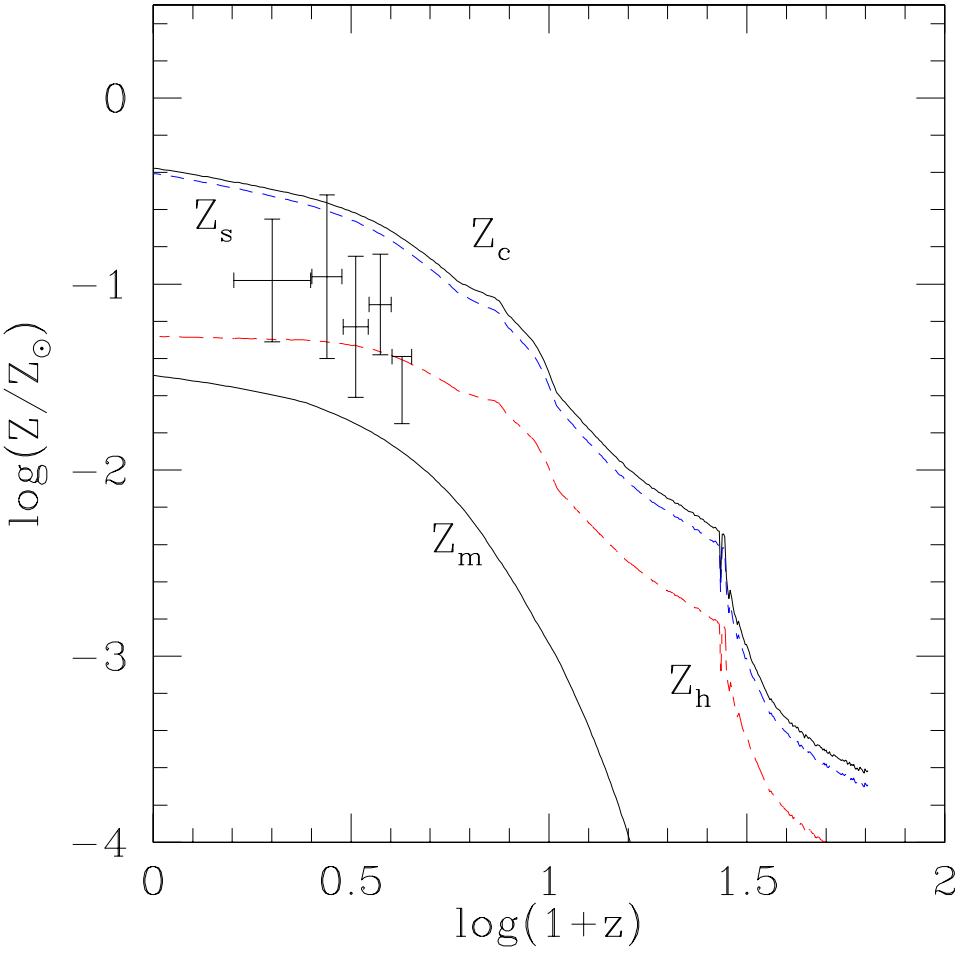

Fig. 11.— Metallicity of various components as a function of redshift.

that, after the Dark Age following recombination at $z \sim 1000$, a phase of galaxy and star formation occurred, followed by radiation emission and subsequent reionization of the Inter Galactic Medium.

Observational constraints on the redshift location of this event have been so far contradictory. On one hand, light coming from distant objects such as Quasi Stellar Objects provides information on the state of the IGM at any successive time. In particular, quasar SDSSp 103027.10+052455.0 at $z = 6.28$ shows evidence of a Gunn-Peterson trough (Becker et al. 2001), the distinctive signature of absorption by neutral hydrogen, implying that reionization occurred at a later time. On the other hand, the results coming from the WMAP mission on the optical depth to electrons of the IGM show that the latter needed to be a ionized plasma already at a much earlier epoch, $z = 20^{+10}_{-9}$ (Bennett et al. 2003).

Several different explanations have been proposed to explain the inconsistency: from the theoretical standpoint, reionization might be a somewhat longer and more complicated transition than traditionally understood. The process can present inhomogeneities, just like the metallicity evolution. Also, two-reionization mechanisms have been proposed (Cen (2002)). Observationally, signatures of a non-uniform reionization may indicate that the QSO result only regards a specific line-of-sight and could be unrelated to the CMB estimate. Needless to say, the availability of GRB data in the redshift interval $5 < z < 20$ could constitute conclusive proof in support of any of these hypotheses.

Fig. 12 illustrates the cosmic history between recombination and the present day, highlighting the candidate redshift span for reionization and the role of GRBs as probes of this phase.

4. Conclusions

We presented a brief overview of the properties and applications of GRB in the cosmological sector. Our task was 2-fold: in the first place, we described the unique features that render GRBs an unique tool for the observational exploration of the early universe, from an exceptional detectability out to very high redshift to a preferred location inside the galactic regions that are undergoing active star formation. In the second place, we analyzed a few potential applications of the GRB data to the study of cosmic evolution.

We have seen how the details of the expansion of the universe can be unveiled by fitting the redshift-magnitude relation to presently avalilable GRB data, constraining both the matter and cosmological constant content of the universe and the equation of state of Dark Energy. We have also seen how GRB data could allow to trace the evolution of

several important entities of our universe: the Star Formation Rate, the metallicity, the reionization. One further potential application, despite the low statistics, is mapping the Large Scale Structure.

All these considerations suggest that forthcoming GRB data could provide an unvaluable and unprecedented insight into cosmic evolution.

REFERENCES

Becker, R.H. et al. 2001, AJ, 122, 2850

Bennett, C.L. et al. 2003, ApJS, 148, 1

Cen, R. 2002, ApJ, 591, 12

Ghirlanda, G., Ghisellini, G. & Lazzati, D. 2004, ApJ, 616, 331

Ghisellini, G. 2004, Int.J.Mod.Phys.A

Gou, L.J. et al. 2004, ApJ, 604, 508

Lamb, Q.D. 2000, Phys.Rep., 333, 505

Lamb, Q.D. & Reichart, D.E. 2001, preprint (astro-ph/0109037)

Lu, L. et al. 1996, ApJS, 107, 475

Matheson, T. et al. 2003, ApJ, 559, 394

Porciani, C. & Madau, P. 2000, ApJ, 548, 522

Stanek, K.Z. 2004, preprint (astro-ph/0411361)

This preprint was prepared with the AAS LaTeX macros v5.2.

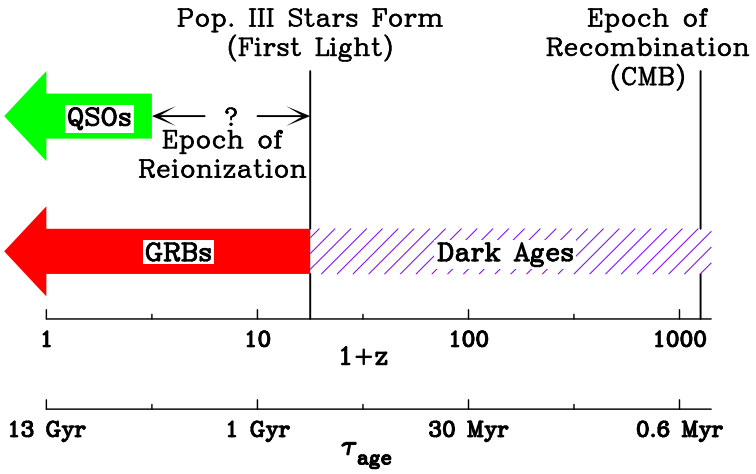

Fig. 12.— Redshift span of the reionization history of the universe.